Controls on sublithospheric small-scale convection

Jinshui Huang, Shijie Zhong, and Jeroen van Hunen
Department of Physics, University of Colorado at Boulder, Boulder, Colorado, USA

Received 17 February 2003; revised 5 June 2003; accepted 10 June 2003; published 30 August 2003.

[1] The Pacific upper mantle structures revealed from recent seismic studies prompt us to study the dynamics of sublithospheric small-scale convection (SSC) derived from thermal boundary layer instabilities of cooling lithosphere. As oceanic lithosphere cools and thickens, its sublayer may go unstable, thus producing SSC in the asthenosphere. By formulating two-dimensional (2-D) and three-dimensional (3-D) numerical models with realistic mantle rheology, we examine the controls on the onset time of SSC and its dynamic consequences. The onset of SSC is mainly controlled by two parameters: activation energy and asthenospheric viscosity, which can be recast as the Frank-Kamenetskii parameter θ and a Rayleigh number Ra_i, respectively. Our models show that the onset time of SSC, τ_c, scales as $R\bar{a}_i^{0.68}\theta^{0.74}$, independent of 2-D or 3-D geometry. Our scaling coefficient for θ is significantly smaller than that from previous studies, but the weaker dependence on activation energy confirms the result of *Korenaga and Jordan* [2003]. We found that thermal structure associated with age offset across fracture zones has significant effects on the onset of SSC, and it causes the SSC to occur always first near the fracture zones. Asthenospheric thickness and plate motion may also have significant effects on the onset of SSC. When the thickness of asthenosphere is sufficiently small to be comparable with the wavelength of the SSC, the onset may be delayed significantly. Plate motion also tends to delay the onset of the SSC in our 2-D models. Although at the onset of SSC surface heat flux Q is consistent with the half-space cooling model prediction, Q may eventually deviate from the half-space cooling model prediction as thermal perturbations associated with SSC diffuse through the stable part of lithosphere or stagnant lid to the surface. We found that the time it takes for Q to deviate from the half-space cooling model after the onset of SSC, $\Delta\tau$, scales as $R\bar{a}_i^{0.65}\theta^{1.52}$, while the thickness of the stagnant lid at the onset time, δ, scales as $R\bar{a}_i^{0.33}\theta^{0.78}$, which is consistent with $\Delta\tau \sim \delta^2$ for thermal diffusion. At the onset of SSC, Q scales as $Ra_i^{0.34}\theta^{-0.37}$ or $\tau_c^{-0.5}$ as expected from the half-space cooling model. However, these scaling coefficients change significantly with time. After nine onset times Q scales as $Ra_i^{0.28}\theta^{-0.7}$, which although showing the trend toward the scaling for steady state convection is still far from the predictions for steady state convection, thus suggesting a fundamentally transient nature of the SSC. *INDEX TERMS:* 8120 Tectonophysics: Dynamics of lithosphere and mantle—general; 8121 Tectonophysics: Dynamics, convection currents and mantle plumes; 8162 Tectonophysics: Rheology—mantle

Citation: Huang, J., S. Zhong, and J. van Hunen, Controls on sublithospheric small-scale convection, *J. Geophys. Res.*, *108*(B8), 2405, doi:10.1029/2003JB002456, 2003.

1. Introduction

[2] It has been inferred on the basis of surface observations of plate tectonics and hot spot volcanism that mantle convection may consist of two distinct modes: plate-mode and plume-mode [*Davies and Richards*, 1992]. While plume-mode convection is responsible for hot spot volcanisms [*Morgan*, 1981], plate-mode convection is associated with the creation and subduction of oceanic lithospheres or plates, one of the most important physical processes governing the thermal evolution of the mantle. Both the plate-mode and plume-mode result from gravitational instabilities of thermal boundary layers (TBLs). Mantle plumes result from instabilities of the bottom TBL (e.g., core-mantle boundary). Oceanic lithosphere is the top TBL of mantle convection. Subduction of oceanic lithosphere may be considered as instabilities of the top TBL as the cooling of lithosphere causes the lithospheric buoyancy to increase to a critical level [*McKenzie et al.*, 1974], although highly nonlinear deformational mechanisms including faulting and/or plasticity are also essential for subduction [*Zhong and Gurnis*, 1996; *Bercovici*, 1998; *Tackley*, 2000; *Moresi and Solomatov*, 1998; *Conrad and Hager*, 1999].

[3] In addition to plate-mode and plume-mode convection, another mode of convection, namely sublithospheric small-scale convection (SSC), has also been proposed [*Richter*, 1973; *Richter and Parsons*, 1975; *Parsons and*

0148-0227/03/2003JB002456$09.00

McKenzie, 1978]. The SSC is caused by the same physical mechanism (i.e., instabilities of TBL) as that for plate-mode and plume-mode convection. The SSC occurs in the bottom portion of oceanic lithosphere where the superadiabatic temperature and relatively small viscosity cause the convective instabilities. The SSC was originally proposed mainly to explain the reduced subsidence of seafloor topography and the constancy of heat flux at relatively old seafloor [*Parsons and McKenzie*, 1978], both representing significant deviations from the half-space cooling model that predicts well the seafloor topography and heat flux at young seafloors [*Parsons and Sclater*, 1977; *Turcotte and Schubert*, 1982; *Lister et al.*, 1990]. Later, it was suggested that the SSC be responsible for the undulation of short-wavelength (~300 km) geoid in the Pacific [*Buck*, 1985; *Buck and Parmentier*, 1986; *Haxby and Weissel*, 1986].

[4] Recently, seismic studies reveal small-scale structures in the Pacific upper mantle [*Katzman et al.*, 1998; *Chen et al.*, 2001; *Montagner*, 2002] and age-dependent lithospheric thermal structures that differ from the half-space cooling model prediction at relatively old seafloors [*Ritzwoller et al.*, 2002]. These studies suggest that the SSC may be responsible for producing the seismic structures [e.g., *Katzman et al.*, 1998]. While previous seismic studies have focused on the large-scale structures in the lower mantle that are largely related to the plate-mode convection (i.e., plate subduction) [e.g., *Van der Hilst et al.*, 1997; *Grand*, 1994], these more recent seismic studies on the oceanic upper mantle structure [*Katzman et al.*, 1998; *Ritzwoller et al.*, 2002; *Montagner*, 2002] help understand the dynamic interaction between oceanic lithosphere and the upper mantle and the nature of the SSC.

[5] The SSC has been studied previously with both numerical and laboratory simulations [*Davaille and Jaupart*, 1993, 1994; *Buck and Parmentier*, 1986; *Yuen and Fleitout*, 1985; *Ogawa et al.*, 1991; *Dumoulin et al.*, 2001; *Marquart*, 2001; *Korenaga and Jordan*, 2002a, 2003]. The focuses of these studies include the onset time of the SSC and the subsequent evolutions of surface heat flux [*Davaille and Jaupart*, 1994], gravity anomalies [*Buck and Parmentier*, 1986], and structural wavelengths of the SSC [*Robinson et al.*, 1987]. More recent studies have taken into account realistic temperature-dependent Newtonian rheology. In their laboratory studies, *Davaille and Jaupart* [1993, 1994] showed that onset time of SSC and the subsequent evolution of surface heat flux are controlled by activation energy E and mantle viscosity η_0. *Davaille and Jaupart* [1994] also suggested that the temperature anomalies of the SSC scale with E^{-1}. With their numerical modeling, *Choblet and Sotin* [2000] developed scaling laws for the onset time of SSC with E and η_0 that are similar to those in the work of *Davaille and Jaupart* [1994]. However, *Korenaga and Jordan* [2002a, 2003] found a much weaker dependence of the onset time on E through both numerical studies and scaling analyses.

[6] In this study, we explore the dynamics of the SSC by focusing our efforts on the following aspects. First, we examine the effects of layered temperature-dependent viscosity on the SSC. Most of the previous studies ignored the layered asthenospheric and upper mantle viscosity structure [e.g., *Davaille and Jaupart*, 1994; *Korenaga and Jordan*, 2003], although it represents an important feature of mantle viscosity structure [*Hager and Richards*, 1989]. Second, we investigate the effects of initial thermal structure on the SSC. In particular, we study how thermal structure associated with transform faults and fracture zones may influence the development of the SSC. Third, we study the effects of plate motion on the onset of the SSC. Previous studies have largely ignored plate motion by focusing on development of the SSC in either a two-dimensional (2-D) plane that is perpendicular to plate motion [*Buck and Parmentier*, 1986; *Robinson et al.*, 1987; *Korenaga and Jordan*, 2003] or a three-dimensional (3-D) box with a pinned top surface [*Davaille and Jaupart*, 1993; *Choblet and Sotin*, 2000]. Fourth, we examine the transient nature of the SSC, in particular, the time dependence of the scaling coefficients of surface heat flux and temperature anomalies in the upper mantle, considering that previous studies model the SSC either with a statistically steady state convection [e.g., *Solomatov and Moresi*, 2000] or convection at the onset time [e.g., *Korenaga and Jordan*, 2002a]. Finally, we reexamine the scaling analyses by *Davaille and Jaupart* [1994] and *Choblet and Sotin* [2000] to understand why their studies produce a much stronger dependence of onset time on activation energy than that reported in the work of *Korenaga and Jordan* [2003].

[7] We organize the paper as follows. In the next section, we will present the model formulation including initial and boundary conditions and rheological equations. We will then systematically examine the controls on the onset of the SSC from mantle rheology to initial conditions, and to plate motion. We then investigate the consequence of the SSC on surface heat flux and upper mantle thermal structure. We will discuss the relevance and limitation of our results before presenting conclusions in the last section.

2. Model Description

[8] In this study, we mainly use two different types of 2-D models to investigate the SSC: longitudinal roll (LR) and transverse roll (TR) models (Figure 1). The LR models are used to examine the SSC in a 2-D plane that is perpendicular to plate motion, while the TR models are used to study the SSC in a 2-D plane that is parallel to plate motion and with velocity imposed on top. With our 2-D approximation, the LR models imply that SSC associated with the instabilities of TBLs produce convective rolls aligned with plate motion (i.e., LRs or Richter rolls), while SSC in the TR models generates convective rolls perpendicular to plate motion (TRs) [e.g., *Davies*, 1988]. The basic physical process of the instabilities of TBLs can be described as follows [*Davaille and Jaupart*, 1994]. The cooling at the surface leads to thickening of the top TBL. The top TBL eventually goes unstable when its thickness increases to a value such that the local Rayleigh number is larger than a critical Rayleigh number. This process can be described by the conservation equations of mass, momentum, and energy. With the assumption of an incompressible mantle and Boussinesq approximation, the nondimensional governing equations are given as [*McKenzie et al.*, 1974]

$$\nabla \cdot \mathbf{u} = 0, \tag{1}$$

$$-\nabla P + \nabla \cdot \left[\eta\left(\nabla \mathbf{u} + \nabla^T \mathbf{u}\right)\right] + RaTe_z = 0, \tag{2}$$

$$\frac{\partial T}{\partial t} + \mathbf{u} \cdot \nabla T = \nabla^2 T, \tag{3}$$

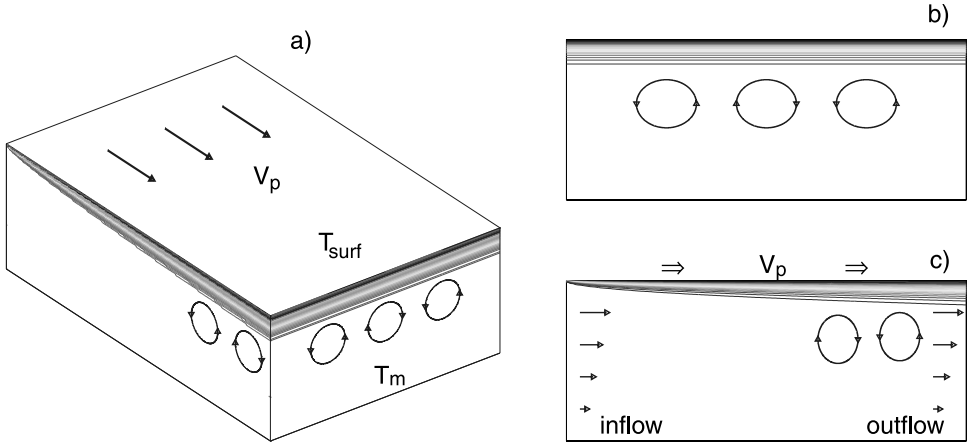

Figure 1. Schematic diagrams of the oceanic mantle below a moving plate (a) and two types of 2-D models employed in this study: LR model (b) and TR model (c).

where **u**, P, η, and T are velocity, pressure, viscosity, and temperature, respectively; e_z is the unit vector in vertical direction, and Ra is a Rayleigh number that is defined as

$$Ra = \frac{\alpha\rho_0 g\Delta T D^3}{\kappa\eta_0}, \tag{4}$$

where α is the coefficient of thermal expansion, ρ_0 is the reference mantle density, η_0 is the reference viscosity that is taken as the viscosity at the bottom boundary unless otherwise indicated, D is the thickness of the box, κ is the thermal diffusivity, ΔT is the temperature difference across the box, and g is the gravitational acceleration. Equations (1)–(3) are obtained by using the following characteristic scales: length $[L] = D$; time $[t] = D^2/\kappa$; viscosity $[\eta] = \eta_0$; and temperature $[T] = \Delta T$. The relevant model parameters are given in Table 1.

[9] We assume a Newtonian rheology for the mantle with the Arrhenius rheology law. The viscosity in dimensionless form is

$$\eta = \eta_r \exp\left(\frac{E}{T + T_{\text{off}}} - \frac{E}{1 + T_{\text{off}}}\right), \tag{5}$$

where $\eta_r = \eta_b/\eta_0$, $\eta_r = 1$ for most cases as η_b is the viscosity at the bottom boundary, $T_{\text{off}} = T_s/\Delta T$, E is nondimensional activation energy and is related to activation energy E^* as $E = E^*/(R\Delta T)$ with R as the gas constant, and T_s is the surface temperature and is 273 K. We impose a cutoff of 10^6 for viscosity in our models.

[10] For the LR models, the boundary conditions for temperature are $T = 0$ and 1 for the top and bottom boundaries, respectively, and vanishing heat flux for the sidewalls. The boundary conditions for velocity are no slip at the top boundary and free slip on all the other boundaries. The temperature is initially equal to 1 everywhere (i.e., lithosphere with a zero age). Superimposed on this initial temperature is a randomly perturbed temperature of amplitude δT (10^{-3} for most cases).

[11] The TR models use flow-through boundary conditions (Figure 1). While the temperatures at the top and bottom boundaries are 0 and 1, respectively, $\partial T/\partial x = 0$ for the outflow boundary and $T = T_0(z, t_0) + \delta T$ for the inflow boundary, where $T_0(z, t_0)$ is the temperature at depth z predicted from the half-space cooling model [e.g., *Turcotte and Schubert*, 1982] for lithospheric age t_0, and δT is the small random perturbation (10^{-3}). The top boundary is prescribed with a plate velocity V_p, while the bottom boundary is fixed. The horizontal velocity at the inflow and outflow boundaries $V_b(z)$ is the velocity of a Couette flow [*Turcotte and Schubert*, 1982] for a variable viscosity fluid. The initial temperature is derived from the half-space cooling model. However, our results from TR models are insensitive to initial conditions because the models are computed to a steady state.

[12] The governing equations with variable viscosity are solved with a finite element code Citcom [*Moresi and Solomatov*, 1995; *Moresi and Gurnis*, 1996] with some extensions [*Zhong et al.*, 2000]. For most of the LR models, we use a box with aspect ratio of 3 and 192 × 96 finite elements, but different aspect ratios are also used to investigate the effects of box size. The aspect ratio for our TR models is 12 with 384 × 64 finite elements. The elements are refined near the boundary layer to better resolve the development of the TBL instabilities.

[13] In addition to these 2-D models, we have also computed a set of 3-D models to examine to what extent our 2-D results are sensitive to 3-D effects. The 3-D models are done in a unit cube with 64 × 64 × 64 elements, and they are identical to 2-D LR models except the geometry.

3. Results

[14] Two important parameters in our models are nondimensional activation energy E and Rayleigh number Ra. In

Table 1. Physical and Geometrical Model Parameters

Parameter	Value
Thickness of the box (D)	10^6 m
Temperature drop of the layer (ΔT)	1350 K
Reference density (ρ_0)	3.3×10^3 kg m^{-3}
Thermal diffusivity (κ)	10^{-6} m^2 s^{-1}
Heat conductivity (k)	3.2 W m^{-1} K^{-1}
Coefficient of thermal expansion (α)	2×10^{-5} K^{-1}
Acceleration of gravity (g)	10 m s^{-2}
Gas constant (R)	8.31 J mol^{-1}

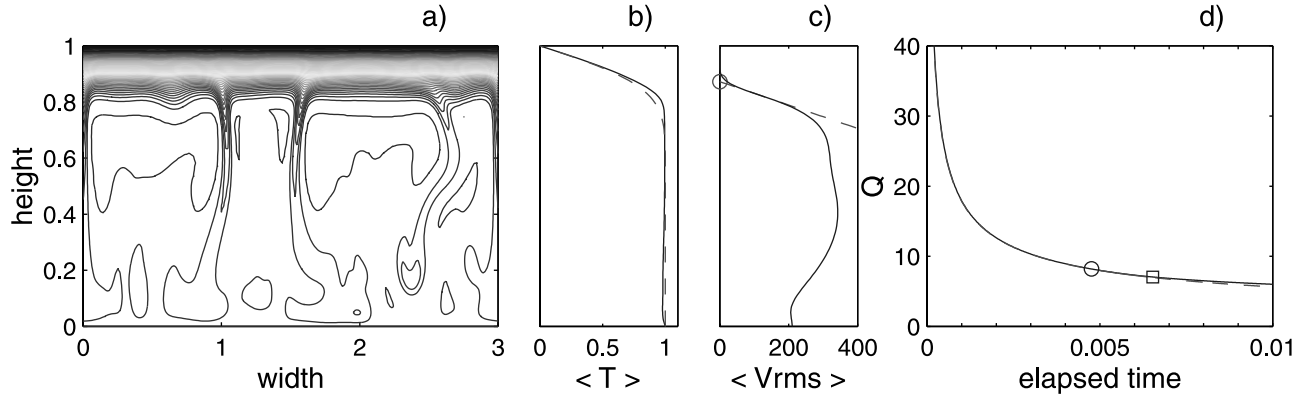

Figure 2. A representative temperature field after the TBL instability starts (a), the corresponding horizontally averaged temperature (b), RMS velocity (c), and time-dependent surface heat flux (d). In Figures 2b and 2d, the dashed lines represent the predictions from the half-space cooling model. In Figure 2d, the square indicates the time at which (a), (b), and (c) are taken, and the circle shows the onset time for this case. The thickness of stagnant lid is determined from the RMS velocity profile.

this section, we will study how the development of SSC depends on these two parameters. Our focus is on the SSC in the LR models (i.e., in a plane perpendicular to plate motion) and how stratified viscosity, aspect ratio of the box, initial thermal structure including that associated with fracture zones, and plate motion influence the SSC. We will derive scaling laws that describe dependences of the SSC on input parameters. However, instead of using E and Ra in our scaling laws, following that in the work of *Solomatov and Moresi* [2000], we scale our results in terms of Rayleigh number defined by viscosity at interior temperature T_i, Ra_i, and the Frank-Kamenetskii parameter θ that is defined as

$$\theta = -\frac{\partial(\ln \eta)}{\partial T}\bigg|_{T=T_i} = \frac{E}{(T_i + T_{\text{off}})^2}, \tag{6}$$

where T_i is obtained by averaging the temperature over the box excluding the top and bottom boundary layers.

3.1. Onset Time of the SSC

[15] We first study the onset time of the SSC from 20 LR model calculations with E varying from 5.35 to 32.10 (or E^* from 60 to 360 kJ mol^{-1}), Ra varying from 10^6 to 10^8, and aspect ratio of 3 (see Table 1 for other parameters). The initially uniformly hot fluid cools from the surface with time. As the top TBL increases in thickness, the bottom part of the TBL eventually goes unstable and generates cold downwellings. The temperature field, horizontally averaged temperature and RMS velocity, and time-dependent surface heat flux for a case with $E = 10.70$ and $Ra = 10^7$ after the SSC starts are shown in Figure 2. We adopt the criterion used by *Davaille and Jaupart* [1993] to determine the onset of the SSC. The onset time is defined as the time at which the horizontally averaged temperature starts to deviate from the half-space cooling model prediction by more than 1% at any depth. Different criteria may lead to different onset times. However, we found that the scaling coefficients in our scaling laws for onset time are rather insensitive to the choice of the criteria.

[16] Our measurements of onset times for different E and Ra are summarized in Figures 3a–3c. Because the cooling of the interior is insignificant at the onset, the interior temperature T_i is nearly the same as the initial interior temperature (i.e., 1). Therefore Ra_i is identical to Ra, and θ is linearly proportional to E (equation (6)). The results show that the onset time increases with θ or activation energy and decreases with Rayleigh number. The onset time τ_c scales as follows:

$$\tau_c = (62.6 \pm 1.7) Ra_i^{-0.68\pm0.01} \theta^{0.74\pm0.03}. \tag{7}$$

Here the uncertainties given for the scaling coefficients reflect how well the scaling law fits the numerical results of τ_c. We realize that other random processes occurring naturally in any fluid flow may result in larger uncertainties in the onset time [e.g., *Davaille and Jaupart*, 1994].

[17] With this scaling law, $\tau_c = 50$ Ma would require that asthenospheric viscosity be 1.67×10^{19} Pa s for activation energy of 180 kJ mol^{-1}. The scaling with Ra_i (Figure 3a) is similar to that from laboratory experiments and scaling analysis in the work of *Davaille and Jaupart* [1994] and *Choblet and Sotin* [2000], but the scaling with θ (Figure 3b) is significantly smaller than 8/3 suggested in the work of *Davaille and Jaupart* [1994] and *Choblet and Sotin* [2000]. The weaker dependence of onset time on activation energy is consistent with the finding by *Korenaga and Jordan* [2003] who also discussed the potential causes for the discrepancy, which we will discuss later.

[18] In all our models, surface heat flux follows the half-space cooling model prediction for a period of time even after the onset of SSC (Figure 2d). When surface heat flux starts to deviate from the half-space cooling model (Figure 2d), the downwellings have well developed (Figure 2a). We may define another onset time τ_f as the time at which the surface heat flux starts to deviate from the half-space cooling model by more than 1%. We introduce a new measure, differential onset time $\Delta\tau$ as $\Delta\tau = \tau_f - \tau_c$. We found that $\Delta\tau$ scales as $\Delta\tau = (2.94 \pm 0.16) Ra_i^{0.65\pm0.03} \theta^{1.52\pm0.05}$ (Figure 3d). The scaling coefficient for Ra_i is similar to that for onset time τ_c, but the scaling for θ is rather different.

[19] This delay in observing heat flux deviation from the half-space cooling model has also been reported in the work of *Davaille and Jaupart* [1994] and *Choblet and Sotin*

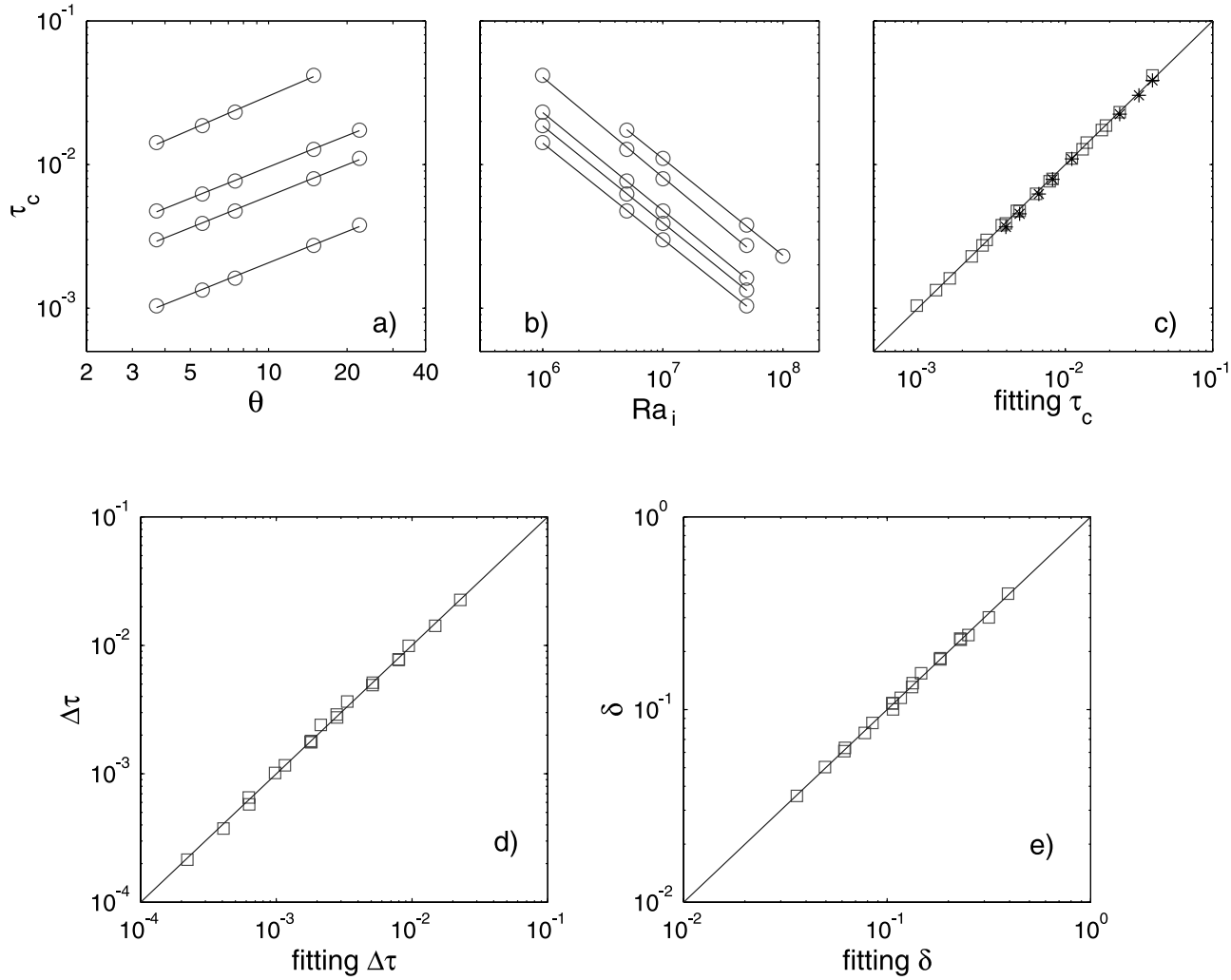

Figure 3. Onset times τ_c from 2-D LR models with different activation energy E and Rayleigh number Ra scale with θ (a) and Ra_i (b), their fitting to the scaling law (c), the fittings to scaling laws of differential onset time $\Delta\tau$ (d), and stagnant lid thickness δ at the onset time (e). The squares and stars in Figure 3c are from 2-D LR and 3-D models, respectively.

[2000] who attribute the delay to the effects of thermal diffusion through the rigid lithosphere. To test this idea, we examine the θ- and Ra_i-dependence of the stagnant lid thickness δ at the onset. Here δ is determined with the horizontally averaged RMS velocity, that is, in the RMS velocity profile, δ is the depth at which the tangential line with the maximum gradient intersects with the vertical axis (Figure 2c) [*Solomatov and Moresi*, 2000]. We find that at the onset time $\delta = (4.73 \pm 0.13)Ra_i^{0.33\pm0.01}\theta^{0.78\pm0.02}$ (Figure 3e). The scaling coefficients for δ are approximately half of those for $\Delta\tau$. This suggests that $\Delta\tau \sim \delta^2$, thus confirming the control of thermal diffusion on the delay in observing heat flux deviation from the half-space cooling.

3.2. Effects of Aspect Ratio of the Box and Stratified Viscosity

[20] E and Ra control not only the onset time but also the wavelength of the SSC. When the wavelength of SSC is comparable to the thickness of the box, the onset time may be affected by boundary conditions imposed at the sidewalls. For the same reason, the thickness of the asthenosphere may also influence the onset time of SSC, as the SSC is largely confined within the asthenosphere [*Robinson et al.*, 1987]. Here we examine the effects of asthenospheric thickness and aspect ratio of the box on onset time.

[21] We first repeat the cases in section 3.1 but with an aspect ratio of 1 instead of 3. We find the following scaling for onset time $\tau_c' \propto Ra_i^{0.73}\theta^{0.75}$. The scaling with θ is nearly the same as that for aspect ratio of 3, but the scaling with Ra_i is slightly larger. We find that for cases with small Ra and/or large E (i.e., relatively large onset time), onset times from models with aspect ratio of 1 tend to be larger than those with aspect ratio of 3. This arises because at small Ra and/or large E, the wavelength of SSC is relatively large and can be comparable with the box size for aspect ratio of 1.

[22] We then compute the above cases using a box with aspect ratio of 6. We find that the onset time τ_c'' is nearly identical to that with aspect ratio of 3. This indicates that aspect ratio of 3 is sufficient for determining the onset for the model parameters considered in this study.

[23] Next we study the effects of stratified viscosity structure on onset time of SSC. To simulate the stratifica-

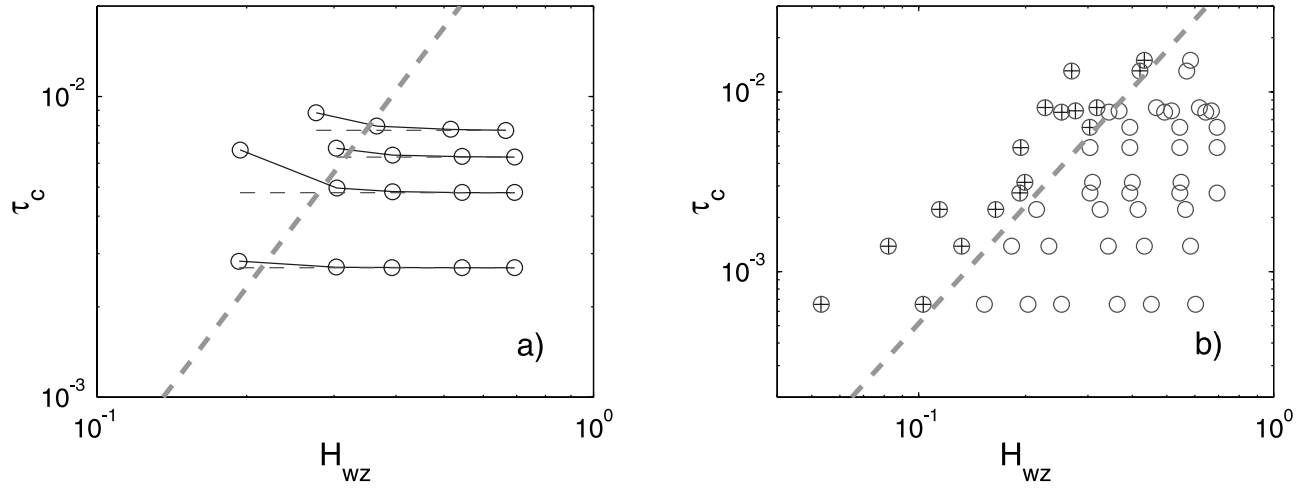

Figure 4. The dependence of onset time τ_c on asthenospheric thickness H_{wz} for models with four different pairs of E and Ra (a) and for models with more densely sampled model parameters (b). In Figure 4a, the thin dashed lines show the reference onset times with no stratified viscosity. In Figure 4b, the circles are for cases in which the delay in onset time is less than 5%, while the circles with a cross sign represent those cases in which the delay is more than 5%. The thick dashed lines represent the dependence of the critical thickness H_{wz}^c on τ_c.

tion, we divide the box into two layers in which the viscosity for the bottom layer is 60 times that for the top layer (i.e., η_r in equation (5) is 60 for the bottom layer, while it remains 1 for the top layer). The thickness of the top layer is H. We examine the effects of stratified viscosity by varying H from 0.1 to 0.8 and comparing the resulting onset time with that with no stratified viscosity structure. Figure 4a shows the variations of τ_c with H_{wz} for four pairs of E and Ra ([10.70, 5×10^6], [5.35, 5×10^6], [10.70, 10^7], and [21.40, 5×10^7]), where Ra is defined by the reference viscosity in the weak layer, H_{wz} is the thickness of the weak zone in the top layer, and $H_{wz} = H - \delta$, and δ is the stagnant lid thickness determined in the last section. Onset time τ_c increases with decreasing H_{wz}, but the influence of H_{wz} on τ_c is not uniform. For models with E and Ra that lead to small τ_c, H_{wz} needs to be sufficiently small to produce a significant delay for the onset (Figures 4a and 4b). Smaller τ_c occurs for models with larger Ra or smaller E (equation 7) that also tends to produce shorter wavelength structure for the SSC. However, unless H_{wz} is so small that it becomes comparable with the wavelength of the SSC, H_{wz} would not affect τ_c. We define a critical asthenospheric thickness H_{wz}^c as the thickness that leads to 5% delay in the onset, compared to that from the case with no strong bottom layer. H_{wz}^c increases with τ_c according to $H_{wz}^c = 3.26\tau_c^{0.46}$, as derived from Figure 4b. From the scaling for τ_c, this implies $H_{wz}^c = 21.37\, Ra_i^{-0.31}\theta^{0.34}$.

3.3. Effects of Initial Structure Including Fracture Zones

[24] In our previous models, a random perturbation of $\delta T = 10^{-3}$ was introduced in the initial thermal structure. The initial thermal structure may play an important role in the onset of SSC [e.g., *Jaupart and Parsons*, 1985; *Korenaga and Jordan*, 2003]. Here we consider two different types of initial structures. The first is the magnitude of the random perturbation δT. The second is the thermal structure due to age difference across fracture zones.

[25] Reducing random perturbation δT tends to delay the onset of the SSC [e.g., *Korenaga and Jordan*, 2003]. To quantify the effects of δT on our scaling law, we have computed 19 LR models with $\delta T = 10^{-5}$ with E varying from 5.35 to 32.10 and Ra varying from 10^6 to 5×10^7. The onset time τ_c scales as $\tau_c = (79.6 \pm 2.2) Ra_i^{-0.67\pm0.01}\theta^{0.71\pm0.04}$. Compared to calculations with $\delta T = 10^{-3}$, we find that the onset time τ_c is delayed by ~35% (Figure 5a), but the scaling coefficients for Ra_i and θ are nearly identical (equation (7)).

[26] To examine the effects of fracture zones, we first present a model with $Ra = 5 \times 10^7$ and $E = 16.05$ in which the surface is divided into six segments by five fracture zones, and each segment of the surface has a different surface age (Figure 5b from the left to right, the surface age is 0, 10, 15, 5, 10, and 15 Ma, respectively) that determines the interior temperature below. For this case, the downwellings of the SSC are located near the fracture zones but are slightly shifted to its older side (Figure 5b). We also find that the onset is significantly earlier than that without fracture zones. This suggests that a fracture zone may have a significant influence on the onset of the SSC.

[27] In order to quantify the effects of a fracture zone, we compute models for different E and Ra with only one fracture zone at the middle of the box. The initial lithospheric ages are 0 and t_{offset}, on the left and right sides of the fracture zone, respectively. For a given pair of E and Ra, we compute three cases with t_{offset} that are 10, 20, and 30% of the predicted onset time τ_c from equation (7). For a calculation with $t_{offset} = 20\%\tau_c$, $Ra = 5 \times 10^7$, and $E = 10.70$, Figure 5c shows three distinct zones of instabilities. While the instabilities are about to develop below the younger lithosphere (zone I), the older lithosphere (zone III) is underlain by relatively well-developed instabilities. Below the fracture zone on the older side is a fully developed downwelling (zone II) (Figure 5c).

[28] Now let us examine the onset times in these three different zones. The onset times for zones I and III are determined in the same way as before by comparing the temperatures in these zones with the predictions for the half-space cooling model, but for zone III, the initial lithospheric age t_{offset} needs to be included in the half-space cooling model calculations. The onset time in zone II under the fracture zone is defined as the time at which the horizontally averaged temperature starts to deviate from the purely conduction model prediction by 1% at any depth. Figure 5d presents the onset times for these three different zones for models with $E = 5.35$ and 10.7 and $Ra = 5 \times 10^6$, 10^7, and 5×10^7. Comparing with models without fracture zone, the onset times for young and old lithosphere (i.e., zones I and III) do not show any significant changes (Figure 5d). However, the instabilities develop much earlier in zone II below the fracture zone. The larger t_{offset} is, the earlier the onset is. The onset time is 48, 65, and 75% earlier for t_{offset} equal to 10, 20, and 30%, respectively (Figure 5d). This percentage change in onset time is constant for a given t_{offset}, suggesting that t_{offset} does not affect the scaling coefficients of onset time for θ and Ra_i.

3.4. Effects of Plate Motion

[29] *Richter* [1973] suggested that SSC with the TR and LR represents two different types of convective instabilities and that plate motion tends to favor development of the LRs (i.e., Richter rolls). Most of the previous studies [e.g., *Buck and Parmentier*, 1986; *Robinson et al.*, 1987] on the SSC focused on the development of LRs in a 2-D plane that is perpendicular to plate motion (i.e., our LR model). Some other studies [e.g., *Davies*, 1988; *Doin et al.*, 1997; *Dumoulin et al.*, 2001] investigated the development of TRs beneath a moving plate. *Houseman* [1983] suggested that plate motion may prohibit the development of instabilities associated with TRs. However, no direct attempt was made to compare these two different instabilities, which will be done here in this section.

[30] We employ our TR (i.e., TR) model with flow-through boundary conditions (Figure 1c) to study the effects of plate motion on the onset of SSC with TRs. The flow-through boundary conditions enable us to focus on the development of instabilities of the top TBL with minimum influences from the bottom TBL. In order to resolve the top TBL, the inflow boundary is assumed to have thermal structure predicted from a half-space cooling model for a surface that is 10 Ma old. For most cases, we choose plate velocity such that the instabilities start near the middle of the box (Figure 6b). As a result, plate velocity is different for different cases. Fourteen cases with E varying from 5.35 to 21.40 and Ra varying from 10^6 to 5×10^7 are computed to a statistically steady state. The onset time in our TR model is defined as the lithospheric age at which the vertically averaged temperature of the top one fourth of the box starts to deviate from the half-space cooling model (Figure 6a). Here the top one fourth of the box is used because it characterizes better the variations of temperature in the top TBL. In these models, the onset time is determined by the occurrence of the first downwelling drop. Because the first downwelling drop once initiated may travel with plate for a short time before a new drop can form [e.g., *Dumoulin et al.*, 2001], we determine the onset time by averaging it over a certain period of time after a model is in a statistically steady state.

[31] We found that the onset times from the TR model are, in general, ~20% larger than those predicted from the scaling law (i.e., equation (7)) from the LR models (Figure 6c). However, the onset time does not increase further with plate velocity once it reaches certain value (Figure 6d for cases with $E = 8.025$ and $Ra = 10^7$ but three different plate velocities). That the plate motion leads to larger onset time than that from the LR models is consistent with the suggestion in the work of *Richter* [1973] that the LRs are more unstable than TRs. Our results seem to suggest that plate motion of the first order does not affect the onset of the SSC significantly. However, full assessments of the effects of plate motion would require 3-D calculations and stratified viscosity structure, and we defer them for future studies.

3.5. Surface Heat Flux and Interior Temperature Anomalies and their Time Dependence

[32] The SSC results in temperature anomalies in the mantle and causes the surface heat flux to deviate from the half-space cooling model (Figure 2). Both the temperature anomalies and heat flux are important geophysical observations that may be used to constrain the dynamics of the SSC. Based on their laboratory experiments, *Davaille and Jaupart* [1993, 1994] suggested that the surface heat flux shortly after the onset (e.g., a few onset times) scales with Ra_i as $Ra_i^{1/3}$. However, a fundamental feature of the SSC resulting from instantaneous cooling is its time dependence or transient effects [e.g., *Davaille and Jaupart*, 1994]. Here we quantify the transient effects of the heat flux and temperature anomalies of the SSC for the LR models discussed in section 3.1.

[33] Because the surface heat flux changes with time, we first develop scaling laws for the average surface heat flux at the onset time and in the period of a number of onset times following the onset. We then examine how the scaling coefficients change with time. Here for each case, surface heat flux Q after the onset is averaged over a time interval of each onset time. We found that at the onset time $Q = 0.071 Ra_i^{0.34\pm0.01}\theta^{-0.37\pm0.01}$ (Figure 7a). Notice that the scaling coefficients for Ra_i and θ for surface heat flux Q are approximately half of those for the onset time τ_c in equation (7) but with the opposite sign. This is expected given that at the onset time Q does not deviate yet from the half-space cooling model which predicts $Q \propto 1/\sqrt{\tau_c}$. Our scaling with Ra_i is nearly identical to that in the work of *Davaille and Jaupart* [1994]. However, we found that the scaling coefficients for Q are time dependent (Figure 7b). After about nine onset times, the scaling coefficient for Ra_i decreases from 0.34 to 0.28, while the scaling with θ nearly doubles to -0.7 (Figure 7b). This suggests that with time the dependence of Q on Ra_i becomes weaker while the dependence on θ gets stronger. Based on steady state stagnant-lid convection, *Moresi and Solomatov* [1995] suggested that Q: $Ra_i^{0.20}\theta^{-1}$. Our results show this trend, but the difference remains significant at nine onset times (Figure 7b). Although the actual onset time of the SSC remains largely unconstrained, if it is greater than 20 Ma, our results suggest that the steady state results may not be

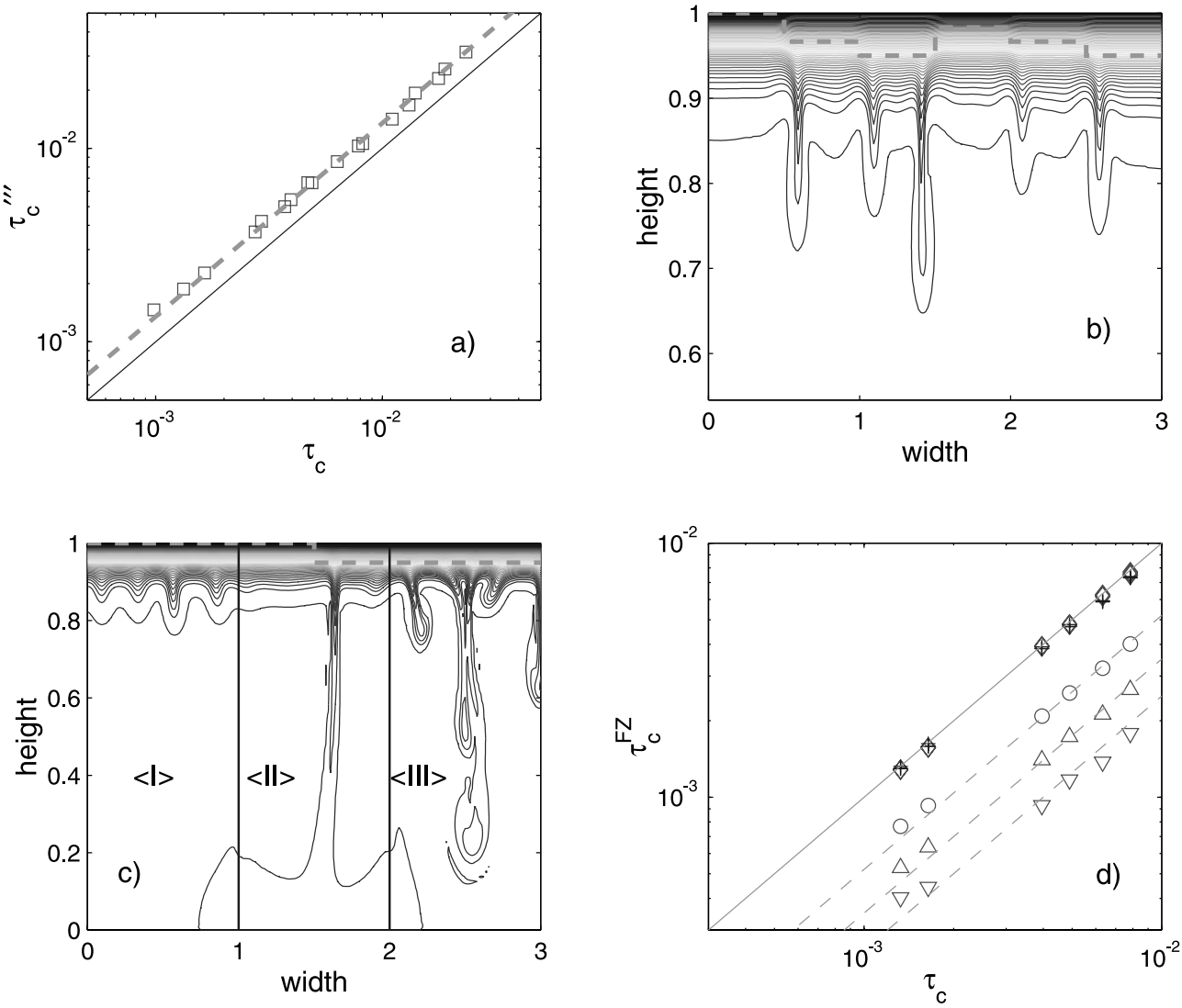

Figure 5. Effects of initial temperature structure on the onset of SSC. Onset time comparison between models with initial perturbation of 10^{-3} (τ_c) and 10^{-5}(τ_c''') (a), representative temperature structure for models with five fracture zones at nondimensional time 9.335×10^{-4} (b), with one fracture zone at nondimensional time 1.546×10^{-3} (c), and the comparisons of onset times τ_c^{FZ} in zones I, II, and III for cases having different age offset across a fracture zone with onset time τ_c with no fracture zone (d). In Figure 5a the dashed line shows τ_c, which is 35% larger than τ_c. In Figures 5b and 5c the thick dashed lines represent the initially different thermal structure due to the age offset. In Figure 5c the vertical lines mark zones I, II, and III. In Figure 5d, models with three different age offsets for each of the six pairs of E and Ra are computed. In Figure 5d, the circles, triangles, and inverted triangles represent the onset times in zone II with age offset of 10, 20, and 30% of τ_c, respectively, and the corresponding dashed line shows τ_c^{FZ}, which is 48, 65, and 75% less than τ_c, respectively. Also, in Figure 5d, the diamonds and crosses represent the onset time τ_c^{FZ} for zones I and III, respectively.

fully applicable for the evolution of the oceanic lithosphere given that the oldest oceanic lithosphere is only ~180 Ma.

[34] We now examine the transient effects of temperature anomalies of the SSC. *Davaille and Jaupart* [1993, 1994] suggested that during the development of the SSC, the temperature difference across the unstable sublayer of the top TBL, ΔT_e, is insensitive to Ra but is inversely proportional to θ. For steady state stagnant-lid convection, *Moresi and Solomatov* [1995] indicated that the temperature difference across the bottom TBL (i.e., $1 - T_i$, where 1 and T_i are the bottom boundary and interior temperatures, respectively) scales as $Ra_i^{-0.04}\theta^{-0.73}$ Here we examine the transient effects of these two temperatures ΔT_e and $1 - T_i$. We determine T_i by averaging the temperature over the box excluding the top and bottom boundary layers where the temperature differs from the interior temperature by more than 5%. However, our determinations of T_i are rather insensitive to this choice (e.g., those in the work of *Moresi and Solomatov* [1995]). In section 3.1, we have determined the thickness of the stagnant lid δ at the onset of the SSC.

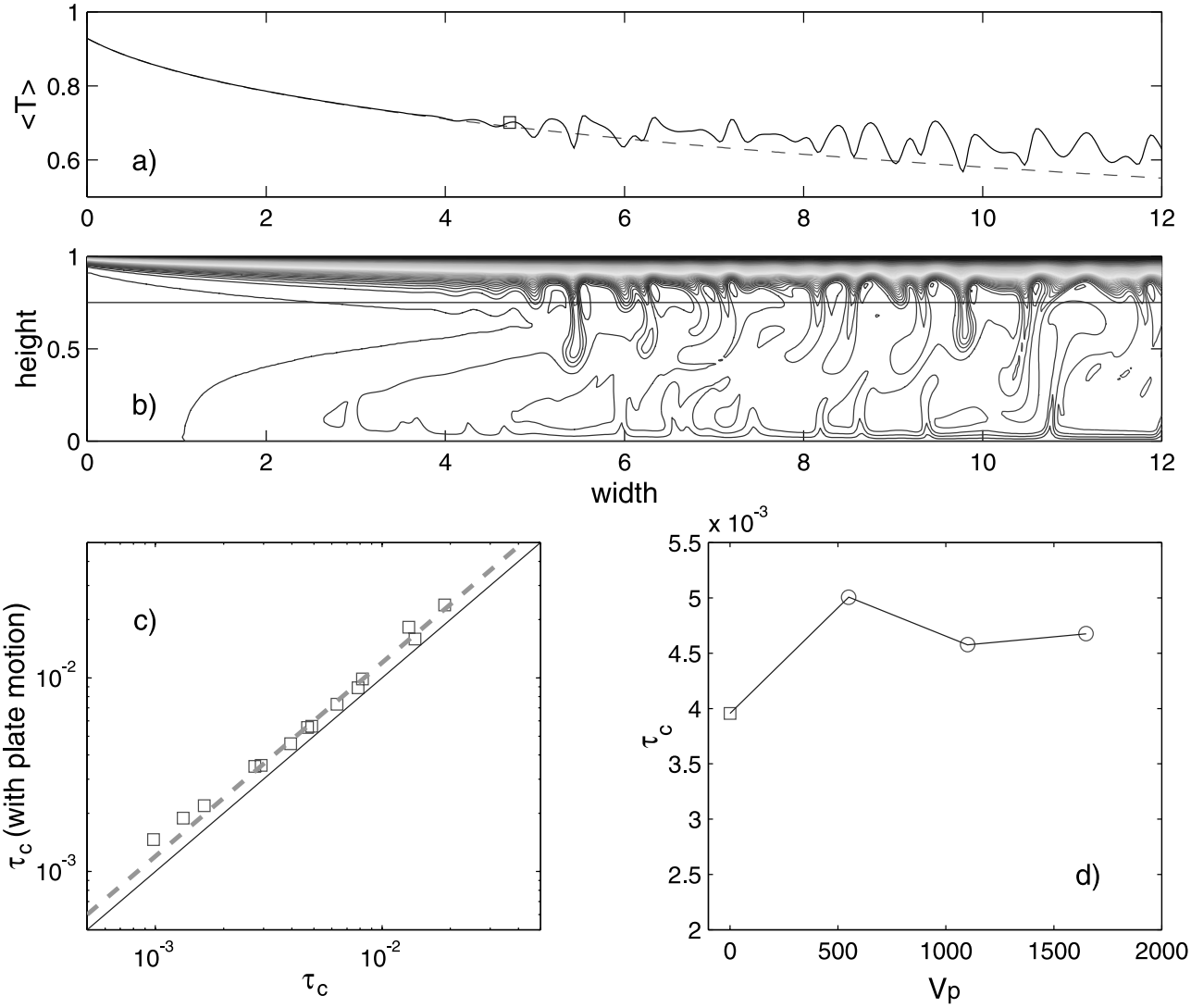

Figure 6. Effects of plate motion on the onset of SSC. The dependence of vertically averaged temperature for the top one fourth of the box for a representative TR model (a), its corresponding temperature structure (b), the comparison of onset time from TR models with different E and Ra with onset time τ_c from the corresponding LR models (c), and the dependence of onset time on plate velocity for $E = 8.025$ and $Ra = 10^7$. In Figure 6a the dash line represents the prediction from the half-space cooling model. In Figure 6c, the dashed line is for onset time with plate motion, which is 20% larger than τ_c from LR models with no plate motion.

From δ we can determine the temperature at the bottom of the stagnant lid, T_{sg}, and then $\Delta T_e = T_i - T_{sg}$. We find that ΔT_e at the onset depends strongly on θ but weakly on Ra_i with the scaling: $\Delta T_e = (1.41 \pm 0.09)\bar{Ra_i}^{0.01\pm0.02}\theta^{-0.82\pm0.06}$ (Figure 8a). The scaling coefficient for θ, -0.82, is smaller than -1.0 as suggested in the work of *Davaille and Jaupart* [1993, 1994].

[35] We use the same method to determine the time-dependent ΔT_e and $1 - T_i$. We find that the scaling coefficients for ΔT_e are moderately time dependent, but the coefficients for $1 - T_i$ show a stronger time dependence (Figures 8b and 8c). The scaling of ΔT_e with Ra_i changes from -0.01 to -0.06, while the scaling with θ changes from -0.82 to -0.68 after nine onset times (Figure 8b). For $1 - T_i$, the scaling coefficient for Ra_i varies from -0.44 to -0.14 and the scaling for θ changes from -0.21 to -0.53 after nine onset times (Figure 8c). Again, these scaling coefficients for $1 - T_i$ approach those from steady state convection, but the difference remains significant after nine onset times (Figure 8c).

4. Discussion

[36] In this study, we examine the controls on the onset of sublithospheric SSC. The onset time of the SSC is mainly controlled by asthenospheric viscosity and activation energy, as suggested by *Davaille and Jaupart* [1994] and *Choblet and Sotin* [2000]. After recasting the asthenospheric viscosity to a Rayleigh number Ra_i and activation energy to the Frank-Kamenetskii parameter θ, we found that the onset time τ_c

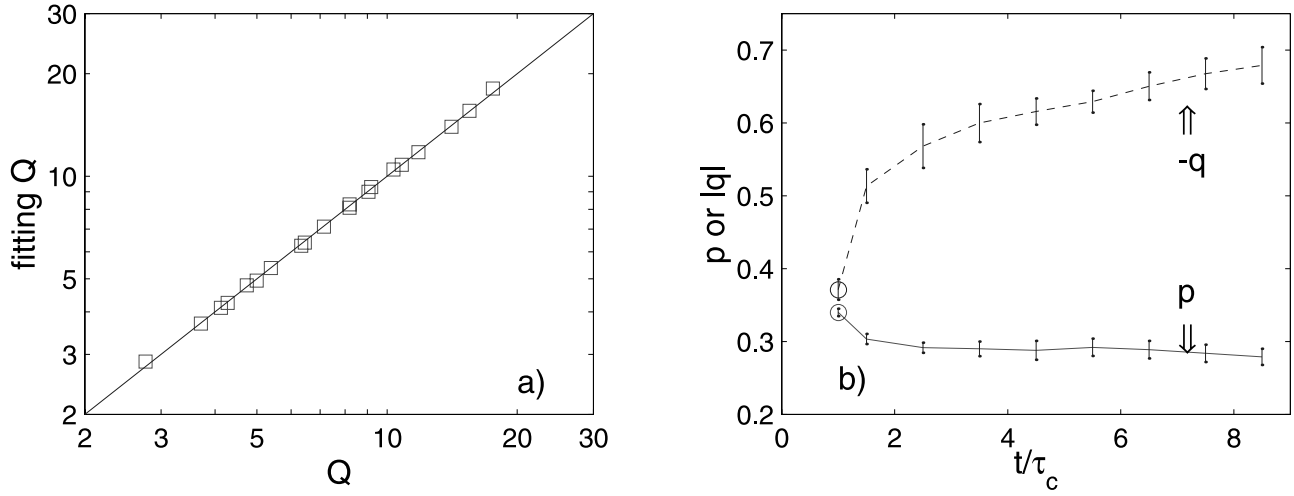

Figure 7. The fitting of averaged surface heat flux Q at onset time to the scaling law (a) and the time dependence of scaling coefficients p and q that are for Ra_i and θ, respectively (b). In Figure 7b, the vertical bars show uncertainties in the scaling coefficients.

scales as $\tau_c = (62.6 \pm 1.7)Ra_i^{-0.68\pm0.01}\theta^{0.74\pm0.03}$. While our scaling coefficient for Ra_i is nearly identical to that in the work of *Davaille and Jaupart* [1994] and *Choblet and Sotin* [2000], the scaling for θ is much smaller than 8/3 suggested in these previous studies. Our result for a weaker dependence of onset time on activation energy is consistent with the finding by *Korenaga and Jordan* [2003].

[37] By using the idea of available buoyancy [*Conrad and Molnar*, 1999] and differential Rayleigh number, *Korenaga and Jordan* [2003] developed a scaling law for onset time that fits their numerical results well. The mathematic form of the scaling law derived by *Korenaga and Jordan* [2003] differs from the polynomial form derived by *Davaille and Jaupart* [1994] in that the effect of activation energy is expressed as a functional, which is related to the available buoyancy. *Korenaga and Jordan* [2003] suggested that the discrepancy between their study and that of *Davaille and Jaupart* [1994] may be caused by a number of potential problems in the work of *Davaille and Jaupart* [1994], including the relatively small viscosity contrast and experimental realizations of the surface cooling and viscosity contrasts in *Davaille and Jaupart*'s [1994] experiments.

[38] Here we point out that a key assumption made in the scaling analyses by *Davaille and Jaupart* [1994] and *Choblet and Sotin* [2000] is invalid, which also contributes to this discrepancy. First, we show that the discrepancy is not caused by model geometries (i.e., 2-D versus 3-D). We have computed eight 3-D models in a unit cube with E varying from 8.025 to 32.1 and Ra varying from 10^6 to 10^7. These 3-D models use the same temperature-dependent viscosity and initial and boundary conditions as those in 2-D LR models. The onset times for these 3-D calculations fit the scaling law of our 2-D LR models well (Figure 3c).

[39] The scaling laws by *Davaille and Jaupart* [1994] and *Choblet and Sotin* [2000] are based on both scaling analyses and model simulations (numerical or laboratory models). The scaling analyses by *Davaille and Jaupart* [1994] and *Choblet and Sotin* [2000] are similar. By assuming that heat flux entering the stagnant lid is provided by the SSC of the unstable sublayer and by using the half-space cooling model for the heat flux at the base of the stagnant lid, one may obtain the following equation, as *Choblet and Sotin* [2000] demonstrated,

$$\tau_c \exp\left(\frac{\delta^2}{2\tau_c}\right) = A\left(\frac{Ra_c}{Ra_i}\right)^{2/3}\left(\frac{\Delta T}{\Delta T_e}\right)^{8/3}, \qquad (8)$$

where Ra_c is a local Rayleigh number, which should be approximately constant at the onset, and A is a constant. This equation was expressed in a slightly different way in the work of *Davaille and Jaupart* [1994] (equation (13)). To derive their scaling laws for τ_c, *Choblet and Sotin* [2000] and *Davaille and Jaupart* [1994] introduced two assumptions to equation (8): (1) $\Delta T_e \sim \theta^{-1}$ and (2) $\exp(\delta^2/2\tau_c)$ is constant and is independent of θ.

[40] In section 3.5, we have seen that at onset time, $\Delta T_e \sim \theta^{-0.82}$ (Figures 8a and 8b), which is generally consistent with the first assumption. However, our numerical results indicate that at the onset $\exp(\delta^2/2\tau_c) \sim \theta^{1.15}$ (Figure 8d), which contradicts the second assumption and is the main cause for the too strong scaling of onset time with θ reported in the work of *Davaille and Jaupart* [1994] and *Choblet and Sotin* [2000]. If at the onset time, equation (8) holds perfectly and Ra_c is constant, our results that $\Delta T_e \sim \theta^{-0.82}$ and $\exp(\delta^2/2\tau_c) \sim \theta^{1.15}$ suggest that $\tau_c \sim \theta$. This is in a reasonable agreement with our scaling $\tau_c \sim \theta^{0.74}$.

[41] Interestingly, it seems that the laboratory results of the onset times by *Davaille and Jaupart* [1994] actually support our scaling for τ_c with a relatively weak dependence on θ. From Figure 4 of *Davaille and Jaupart* [1994], we find that τ_c scales approximately as $\tau_c \sim \theta$. We also notice that the numerical models by *Choblet and Sotin* [2000] investigate only a relatively small range of activation energy (θ varying from 4 to 8), which makes it difficult for accurate scaling analyses. *Korenaga and Jordan* [2003] also suggested that the absence of an initial perturbation in temperature in *Choblet and Sotin* [2000] may have contributed significantly to the discrepancy. However, our calculations

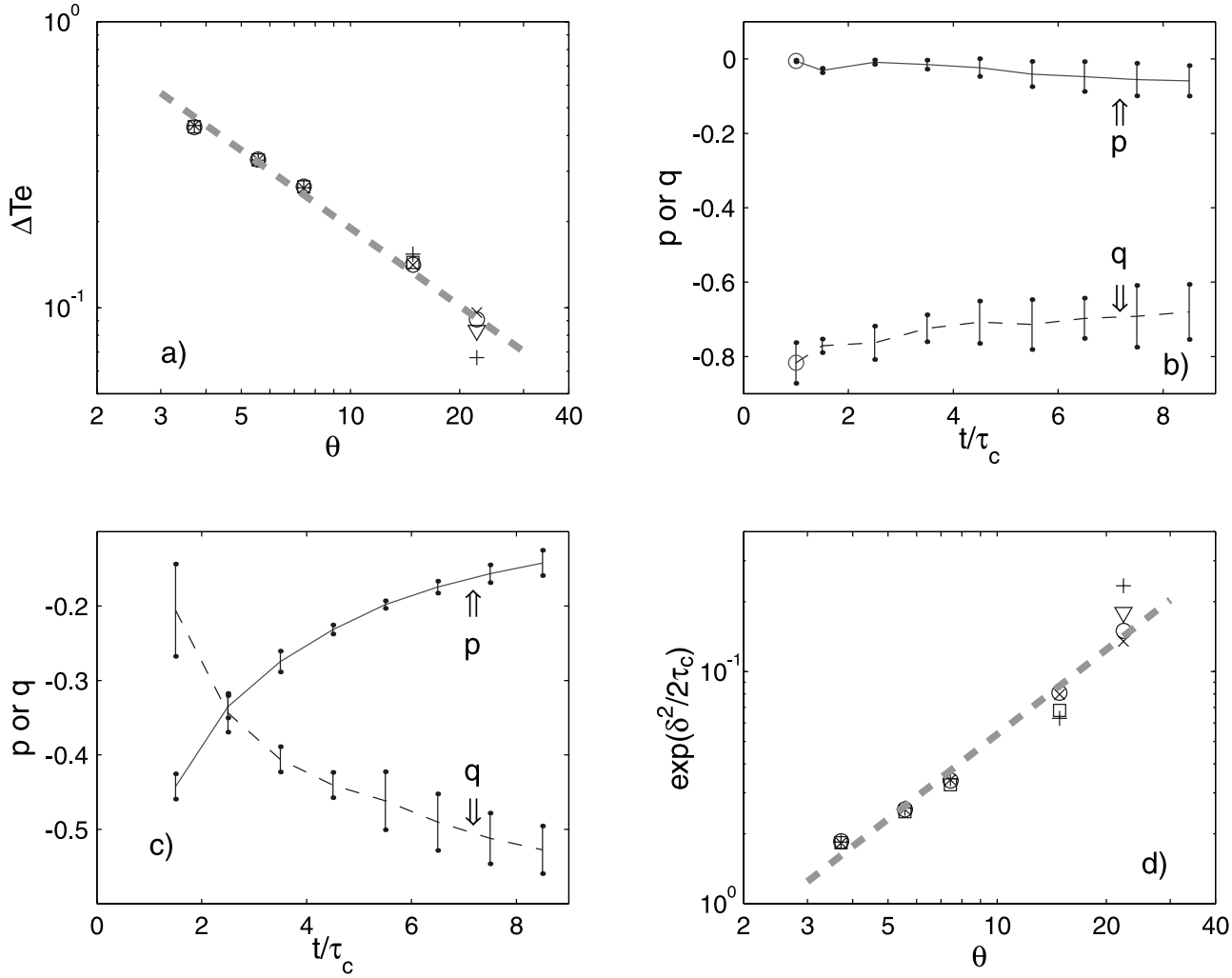

Figure 8. The θ dependence of ΔT_e at onset time for four different *Ra* (a), the time dependence of scaling coefficients p and q that are for Ra_i and θ, respectively, for ΔT_e (b) and $1 - T_i$ (c), and the dependence of $\exp(\delta^2/2\tau_c)$ on θ for four different *Ra* (d). The vertical bars in Figures 8b and 8c show uncertainties in the scaling coefficients.

suggest that while affecting the prefactor of the scaling law for onset time, the initial perturbation does not influence the scaling coefficients on θ and Ra_i (Figure 5a).

[42] In addition to the effects of asthenospheric viscosity and activation energy on the onset of SSC, in this study we also examine the effects of thermal structure associated with fracture zones, the thickness of asthenosphere, and plate motions. Lithosphere may have a quite different age across a fracture zone. This difference in surface age implies a different lithospheric thermal structure across the fracture zone. We found that the SSC always occurs first below fracture zones with downwellings below the older side of the lithosphere across fracture zones due to the difference in thermal structure. This suggests that in seismic studies of oceanic upper mantle structure one should pay more attention to the structure below fracture zones, particularly those with large age offsets, such as the Mendocino fracture zone in the Pacific. Although the thermal structure due to fracture zones promotes the SSC, this structure like initial perturbation to temperature field does not influence the scaling coefficients of the onset time on Ra_i and θ. We also recognize that the effects of fracture zones may be complicated by the dehydration at the mid-ocean ridges that may potentially increase the viscosity for the shallow upper mantle [*Hirth and Kohlstedt*, 1996]. The effect of this increased viscosity as a result of the dehydration was examined in the work of *Korenaga and Jordan* [2002b].

[43] When the thickness of asthenosphere is sufficiently small to be comparable with the wavelengths of the SSC, the onset of SSC may be delayed significantly. Because the wavelengths of the SSC should depend on activation energy and asthenospheric viscosity, we found that the threshold thickness of asthenosphere that would significantly affect the onset time follows the scaling: $H_{\mathrm{wz}}^{c} = 21.37\ Ra_i^{-0.31}\theta^{0.34}$.

[44] Plate motion also tends to delay the onset time in our 2-D TR models. However, for the model parameters that we have considered in this study, plate motion seems to delay the onset time by ~20%, comparing with those from models with no plate motion. *Houseman* [1983] also found with 2-D isoviscous convection models that plate motion tends to delay the development of thermal plumes from the bottom TBL. If we attribute the effects of plate motion to the shear

that it induces, we would anticipate that the effects are larger in the presence of stratified viscosity (e.g., weak asthenosphere), which tends to focus the shear at the shallow depths. On the other hand, 3-D models may also be important in understanding the effects of plate motion on the SSC. This is because plate motion may influence LRs and TRs differently [*Richter*, 1973], while our 2-D TR models only allow us to examine TRs. These potential effects of 3-D geometry and stratified viscosity should be examined in the future studies.

[45] The SSC causes surface heat flux anomalies and thermal structure in the upper mantle, both of which are important geophysical observations. Our studies demonstrate that the 1/3 scaling of heat flux with Ra_i as suggested by *Davaille and Jaupart* [1994] is valid at the onset time when surface heat flux can also be precisely described by the half-space cooling model. After a certain period of time following the onset (depending on the thickness of stagnant lid), the heat flux starts to deviate from the half-space cooling model. However, we found that this 1/3 scaling coefficient with Ra_i decreases with time significantly (Figure 7b). Over a period of nine onset times, this scaling coefficient shows a tendency to approach that suggested for steady state stagnant-lid convection [*Moresi and Solomatov*, 1995]. However, it may take quite a long time to actually reach a steady state. Depending on the actual onset time for the oceanic upper mantle, it is quite possible that the SSC is transient and far from steady state [*Korenaga and Jordan*, 2002a]. We should point out that for certain transient cooling problems, for example, with insulating bottom boundary, steady state scaling laws may still apply if one considers the cooling as the source of internal heating [e.g., *Choblet and Sotin*, 2000].

[46] Similarly, the temperature anomalies associated with the SSC are also time dependent. The temperature anomalies mainly depend on activation energy [*Davaille and Jaupart*, 1994]. However, we found that the scaling coefficient of the temperature anomalies for θ at the onset is only -0.82 and changes to -0.7 after a few onset times (Figure 8b), differing from -1.0 suggested in the work of *Davaille and Jaupart* [1994]. This may have important implications for estimating temperature anomalies in the upper mantle [*Korenaga and Jordan*, 2002a].

5. Conclusions

[47] We have formulated 2-D and 3-D mantle convection models to examine the controls on the onset of sublithospheric SSC and the effects of the SSC on surface heat flux and upper mantle structure. Our models employ a Newtonian rheology with realistic activation energy. Our results can be summarized as follows.

[48] 1. The onset time τ_c of the SSC scales as $\tau_c = (62.6 \pm 1.7)\overline{Ra_i}^{0.68\pm0.01}\theta^{0.74\pm0.03}$, where θ is the Frank-Kamenetskii parameter that depends on the activation energy, and Ra_i is the Rayleigh number that can be related to asthenospheric viscosity. The scaling coefficient for θ is significantly smaller than in the work of *Davaille and Jaupart* [1994] and *Choblet and Sotin* [2000]. The weak dependence of τ_c on activation energy is consistent with that in the work of *Korenaga and Jordan* [2003].

[49] 2. The onset time is sensitive to the initial perturbations, but the scaling coefficients of onset time for Ra_i and θ are not affected. Thermal structure associated with fracture zones on the ocean floors influences the onset in the same way as the initial perturbations. When a fracture zone is present, the SSC always develops first below the fracture zone with a downwelling on the older side of lithosphere across the facture zone.

[50] 3. The onset time is moderately dependent on thickness of asthenosphere and plate motion. When asthenosphere is sufficiently thin such that its thickness is comparable with the wavelength of SSC, we observe significant delays in the onset of SSC. Plate motion tends to moderately delay the onset in comparison with models that do not include plate motion. To fully assess these effects, future studies should employ 3-D models with plate motion and a stratified viscosity structure.

[51] 4. SSC causes surface heat flux Q to be larger than that predicted from the half-space cooling model but only significantly after the onset of SSC. This is because it takes time for the thermal anomalies of the SSC to diffuse through the stable part of the lithosphere (i.e., the stagnant lid). While surface heat flux scales as $Q \approx {Ra_i}^{0.34}\theta^{-0.37}$ at the onset time as expected from $Q \propto 1/\sqrt{\tau_c}$ from the half-space cooling model, this scaling may change significantly with time after the onset. While the scaling coefficients have the tendency to approach those from steady state convection models, they are far from the steady state even after nine onset times. If we attribute the deviation of the heat flux and topography at the seafloor to the SSC, which do not occur until at relatively old seafloor, these results indicate a transient nature of the SSC below oceanic lithosphere.

[52] 5. SSC also induces temperature anomalies in the convective upper mantle. If we define the temperature anomalies as the temperature difference across the unstable sublayer of the top TBL, ΔT_e, we found that ΔT_e is mainly controlled by activation energy and scales as $\overline{Ra_i}^{0.01}\theta^{-0.82}$ at the onset time. The scaling for ΔT_e is also moderately time dependent with the scaling with θ changing from -0.82 to -0.68 after nine onset times.

[53] **Acknowledgments.** We thank P. Molnar and M. Ritzwoller for many stimulating discussions. We also thank V. S. Solomatov for suggesting the use of the Frank-Kamenetskii parameter in our scaling analyses, C. Jaupart for discussions during his visit to University of Colorado at Boulder, and G. Choblet and J. Korenaga for their helpful reviews. This research is supported by David and Lucile Packard Foundation and NSF under grant EAR-0134939.

References

Bercovici, D., Generation of plate tectonics from lithosphere-mantle flow and void-volatile self-lubrication, *Earth Planet. Sci. Lett.*, *154*, 139–151, 1998.

Buck, W. R., When does small-scale convection begin beneath oceanic lithosphere, *Nature*, *313*, 775–777, 1985.

Buck, W. R., and E. M. Parmentier, Convection beneath young oceanic lithosphere: Implications for thermal structure and gravity, *J. Geophys. Res.*, *91*, 1961–1974, 1986.

Chen, L., L. Zhao, and T. H. Jordan, Full three-dimensional seismic structure of the mantle beneath southwestern Pacific ocean, *Eos Trans. AGU*, *82*(47), Fall Meet. Suppl., Abstract [S52F-0699], 2001.

Choblet, G., and C. Sotin, 3D thermal convection with variable viscosity: Can transient cooling be described by a quasi-static scaling law?, *Phys. Earth Planet. Inter.*, *119*, 321–336, 2000.

Conrad, C. P., and B. H. Hager, The thermal evolution of an earth with strong subduction zones, *Geophys. Res. Lett.*, *26*, 3041–3044, 1999.

Conrad, C. P., and P. Molnar, Convective instability of a boundary layer with temperature- and strain-rate-dependent viscosity in terms of 'available buoyancy,' *Geophys. J. Int.*, *139*, 51–68, 1999.

Davaille, A., and C. Jaupart, Transient high-Rayleigh-number thermal convection with large viscosity variations, *J. Fluid Mech.*, *253*, 141–166, 1993.

Davaille, A., and C. Jaupart, Onset of thermal convection in fluids with temperature-dependent viscosity: Application to the oceanic mantle, *J. Geophys. Res.*, *99*, 19,853–19,866, 1994.

Davies, G. F., Ocean bathymetry and mantle convection, 2, Small scale flow, *J. Geophys. Res.*, *93*, 10,481–10,488, 1988.

Davies, G. F., and M. A. Richards, Mantle convection, *J. Geol*, *100*, 151–206, 1992.

Doin, M. P., L. Fleitout, and U. Christensen, Mantle convection and stability of depleted and undepleted continental lithosphere, *J. Geophys. Res.*, *102*, 2771–2787, 1997.

Dumoulin, C., M. P. Doin, and L. Fleitout, Numerical simulations of the cooling of an oceanic lithosphere above a convective mantle, *Phys. Earth Planet. Inter.*, *125*, 45–64, 2001.

Grand, S. P., Mantle shear structure beneath the America and surrounding oceans, *J. Geophys. Res.*, *99*, 11,591–11,621, 1994.

Hager, B. H., and M. A. Richards, Long-wavelength variations in Earth's geoid: Physical models and dynamic implications, *Philos. Trans. R. Soc. London, Ser. A*, *328*, 309–327, 1989.

Haxby, W. F., and J. K. Weissel, Evidence for small-scale mantle convection from Seasat altimeter data, *J. Geophys. Res.*, *91*, 3507–3520, 1986.

Hirth, G., and D. L. Kohlstedt, Water in the oceanic upper mantle: Implications for rheology, melt extraction and the evolution of the lithosphere, *Earth Planet. Sci. Lett.*, *144*, 93–108, 1996.

Houseman, G., Large aspect ratio convection cells in the upper mantle, *Geophys. J. R. Astron. Soc.*, *75*, 309–334, 1983.

Jaupart, C., and B. Parsons, Convective instabilities in a variable viscosity fluid cooled from above, *Phys. Earth Planet. Inter.*, *39*, 14–32, 1985.

Katzman, R., L. Zhao, and T. H. Jordan, High-resolution, two-dimensional vertical tomography of the central Pacific mantle using *ScS* reverberations and frequency-dependent travel times, *J. Geophys. Res.*, *103*, 17,933–17,971, 1998.

Korenaga, J., and T. H. Jordan, On 'steady state' heat flow and the rheology of the oceanic mantle, *Geophys. Res. Lett.*, *29*(22), 2056, doi:10.1029/2002GL016085, 2002a.

Korenaga, J., and T. H. Jordan, Onset of convection with temperature- and depth-dependent viscosity, *Geophys. Res. Lett.*, *29*(19), 1923, doi:10.1029/2002GL015672, 2002b.

Korenaga, J., and T. H. Jordan, Physics of multiscale convection in the Earth's mantle: Onset of sublithospheric convection, *J. Geophys. Res.*, *108*(B7), 2333, doi:10.1029/2002JB001760, 2003.

Lister, C. R. B., J. G. Sclater, E. E. Davis, H. Villinger, and S. Nagihara, Heat flow maintained in ocean basins of great age: Investigations in the north-equatorial west Pacific, *Geophys. J. Int.*, *102*, 603–630, 1990.

Marquart, G., On the geometry of mantle flow beneath drifting lithospheric plates, *Geophys. J. Int.*, *144*, 356–372, 2001.

McKenzie, D. P., J. M. Roberts, and N. O. Weiss, Convection in the mantle: Towards a numerical simulation, *J. Fluid Mech.*, *62*, 465–538, 1974.

Montagner, J. P., Upper mantle low anisotropy channels below the Pacific plate, *Earth Planet. Sci. Lett.*, *202*, 263–274, 2002.

Moresi, L. N., and M. Gurnis, Constraints on the lateral strength of slabs from three-dimensional dynamic flow models, *Earth Planet. Sci. Lett.*, *138*, 15–28, 1996.

Moresi, L. N., and V. S. Solomatov, Numerical investigation of 2D convection with extremely large viscosity variation, *Phys. Fluids*, *9*, 2154–2164, 1995.

Moresi, L. N., and V. S. Solomatov, Mantle convection with a brittle lithosphere: Thoughts on the global tectonics styles of the Earth and Venus, *Geophys. J. Int.*, *133*, 669–682, 1998.

Morgan, W. J., Hotspots tracks and the opening of the Atlantic and Indian ocean, in *The Oceanic Lithosphere*, vol. 7, *The Sea*, edited by C. Emiliani, pp. 443–487, John Wiley, New York, 1981.

Ogawa, M., G. Schubert, and A. Zebib, Numerical simulations of three-dimensional thermal convection in a fluid with strongly temperature-dependent viscosity, *J. Fluid Mech.*, *233*, 299–328, 1991.

Parsons, B., and D. McKenzie, Mantle convection and thermal structure of the plates, *J. Geophys. Res.*, *83*, 4485–4496, 1978.

Parsons, B., and J. G. Sclater, An analysis of the variation of ocean floor bathymetry and heat flow with age, *J. Geophys. Res.*, *82*, 803–827, 1977.

Richter, F. M., Convection and large-scale circulation of the mantle, *J. Geophys. Res.*, *78*, 8735–8745, 1973.

Richter, F. M., and B. Parsons, On the interaction of two scale convection in the mantle, *J. Geophys. Res.*, *80*, 2529–2541, 1975.

Ritzwoller, M. H., N. Shapiro, and W. Landuyt, Two-stage cooling of the Pacific lithosphere, *Eos Trans. AGU*, *83*(19), Spring Meet. Suppl., Abstract [S41A-02], 2002.

Robinson, E. M., B. Parsons, and S. F. Daly, The effects of a shallow viscosity zone on the apparent compensation of mid-plate swell, *Earth Planet. Sci. Lett.*, *82*, 335–348, 1987.

Solomatov, V. S., and L. N. Moresi, Scaling of time-dependent stagnant convection: Application to small-scale convection on Earth and other terrestrial planets, *J. Geophys. Res.*, *105*, 21,795–21,817, 2000.

Tackley, P. J., Mantle convection and plate tectonics: Toward an integrated physical and chemical theory, *Science*, *288*, 3949–3955, 2000.

Turcotte, D. L., and G. Schubert, *Geodynamics: Application of Continuum Physics to Geological Problem*, John Wiley, New York, 1982.

Van der Hilst, R. D., S. Widiyantoro, and E. R. Engdahl, Evidence for deep mantle circulation from global tomography, *Nature*, *386*, 578–584, 1997.

Yuen, D. A., and L. Fleitout, Thinning of the lithosphere by small-scale convective destabilization, *Nature*, *313*, 125–128, 1985.

Zhong, S., and M. Gurnis, Interaction of weak faults and non-Newtonian rheology produces plate tectonics in a 3D model of mantle flow, *Nature*, *383*, 245–247, 1996.

Zhong, S., M. T. Zuber, L. N. Moresi, and M. Gurnis, Role of temperature dependent viscosity and surface plates in spherical shell models of mantle convection, *J. Geophys. Res.*, *105*, 11,063–11,082, 2000.

J. Huang, J. van Hunen, and S. Zhong, Department of Physics, University of Colorado at Boulder, Campus Box 390, Boulder, CO 80309-0390, USA. (szhong@anquetil.colorado.edu)